Small, E. W., & Peticolas, W. L. (1971) *Biopolymers 10*, 1377–1416.
Thomas, G. J., Jr., & Barylski, J. R. (1970) *Appl. Spectrosc. 24*, 463–464.
Thomas, G. J., Jr., & Hartman, K. A. (1973) *Biochim. Biophys. Acta 312*, 311–322.
Thomas, G. J., Jr., & Livramento, J. (1975) *Biochemistry 14*, 5210–5218.
Thomas, G. J., Jr., & Kyogoku, Y. (1977) *Pract. Spectrosc. 1*, 717–872.
Tomasz, M., Olson, J., & Mercado, C. M. (1972) *Biochemistry 11*, 1235–1241.
Tsuboi, M., Takahashi, S., & Harada, I. (1973) in *Physico-Chemical Properties of Nucleic Acids* (Duchesne, J., Ed.) Vol. 2, pp 91–145, Academic Press, New York.
Wolfsberg, M. (1969) *Annu. Rev. Phys. Chem. 20*, 449–478.

Complete Assignment of Carbon Signals in a Stereospecific Peptide via Selective and Single Off-Resonance Proton Decoupling Experiments. Analysis of the Carbon-13 Nuclear Magnetic Resonance Spectrum of Alumichrome at 67.88 MHz†

Antonio De Marco and Miguel Llinás*

ABSTRACT: Polypeptides and proteins in native conformation exhibit ^{13}C NMR spectra which are highly nondegenerate. Assignment of resonances to carbons in particular residues is hence a prerequisite for a structural analysis of the spectroscopic data. For nonprotonated carbonyl carbons, the assignment can be achieved by selective $\{^1H^{\alpha}\}^{13}C'$ ^2J decoupling. Using this method, we have assigned the Orn^1 and Gly^2 carbonyl resonances in alumichrome at 67.9 MHz. We show that a single off-resonance experiment with the decoupling frequency centered in the aliphatic proton spectrum is sufficient to assign unequivocally all the protonated carbon resonances via analysis of the reduced ^1J heteronuclear splittings. Alumichrome thus becomes the first complex polypeptide spin system whose ^1H, ^{15}N, and now ^{13}C nuclear resonances have been fully identified to date. ^{13}C chemical shifts and ^1H–^{13}C spin–spin couplings are discussed in terms of structural strain leading to specific orbital hybridizations and on the basis of polarization effects due to electron density shifts toward hydrogen-bonding and metal-binding sites. A number of $^3J(^{13}C\text{–}C\text{–}C\text{–}^1H)$ coupling constants measured on selected multiplets after resolution enhancement were used to derive the χ-related Karplus relationship

$$^3J(\theta) = (10.2 \cos^2 \theta - 1.3 \cos \theta + 0.2) \text{ Hz}$$

The assignment of signals in NMR spectra is a crucial step for any conformational interpretation of data. Polypeptides in native nonrandom conformations exhibit ^{13}C NMR spectra that reflect the particular structures (Komoroski et al., 1976; Llinás et al., 1976a). This means that ^{13}C spectra cannot be accounted for in terms of a simple addition of the individual residue subspectra; rather, the spectra show a complex dependence on the structural electronic microenvironment at each particular site. In view of the lack of an adequate theory of ^{13}C chemical shifts, assignment of resonances often is a major problem which can be partly overcome by laborious selective isotopic enrichment (Grathwohl et al., 1973; Sogn et al., 1974), by specific chemical modification (Norton & Allerhand, 1976; Dill & Allerhand, 1977), or, as with ^1H NMR (Llinás et al., 1972), by comparative spectroscopy on species-related polypeptides (Packer et al., 1975; Oldfield et al., 1975; Wilbur & Allerhand, 1977). By use of the latter technique on various isomorphic alumichrome homologues which differ in single residue substitutions at sites 2 and 3 (Figure 1), α-carbon resonances of Gly^1, Gly^2, and Gly^3 could be confidently assigned, while the invariant, nonsubstituted ornithyl C^{α} resonances were only tentatively identified on the basis of weak, nearest-neighbor perturbations and correlations with $^1H^{\alpha}$ chemical shifts (Llinás et al., 1976a, 1977a). Thus, although the comparative data enabled classification of groups of resonances in terms of various carbon types (e.g., ornithyl C^{α}'s, C^{β} + C^{γ}'s, C^{δ}'s, etc.), most of the carbon signals remained unassigned. This reflects a weakness of the approach in that critical residues tend to be evolutionarily invariant and thus difficult to identify by comparative spectroscopy.

In the past, we have developed a technique which enables unequivocal assignment of ^{13}C resonances by sequential $^1H\{^{15}N\}$ and $^{13}C\{^{15}N\}$ experiments on uniformly ^{15}N-enriched peptides (Llinás et al., 1977b). This led to a total solution of the difficult problem of assigning resolved carbonyl resonances in alumichrome (Figure 1). Such heteronuclear decoupling experiments were feasible only because the amide proton spectrum had previously been characterized (Llinás et al., 1972); this provided a starting point for identifying ^1J-coupled ^{15}N resonances (Llinás et al., 1976b) and consequently, by an identical procedure, the connected carbonyl ^{13}C signals. Hence, in principle at least, ^{13}C NMR signals can be identified if the spectrum of other spin–spin-coupled heteronuclei has previously been characterized.

The assignment of ^{13}C spectra of molecules of a certain complexity by single-frequency ^1H decoupling can be nontrivial when the proton spectrum is strongly coupled and resonances overlap extensively. Unambiguous interpretations are hard to achieve because multicoupled spin systems often exhibit second-order effects. Under such circumstances, selective decoupling is difficult at low magnetic fields and tedious and intricate at high field strengths. In contrast, off-resonance irradiation causes a reduction of the splittings due to heteronuclear couplings (Ernst, 1966), which are relatively simple to detect and measure. The technique, increasingly applied to simple organic compounds (Tanabe et al., 1971), can be

† From the Istituto di Chimica delle Macromolecole, Consiglio Nazionale delle Ricerche, 20133 Milano, Italy (A.DeM.), and the Department of Chemistry, Carnegie-Mellon University, Pittsburgh, Pennsylvania 15213 (M.Ll.). *Received March 30, 1979.* This research was supported by the donors of the Petroleum Research Fund, administered by the American Chemical Society, and by the Italian National Research Council.

0006-2960/79/0418-3846$01.00/0

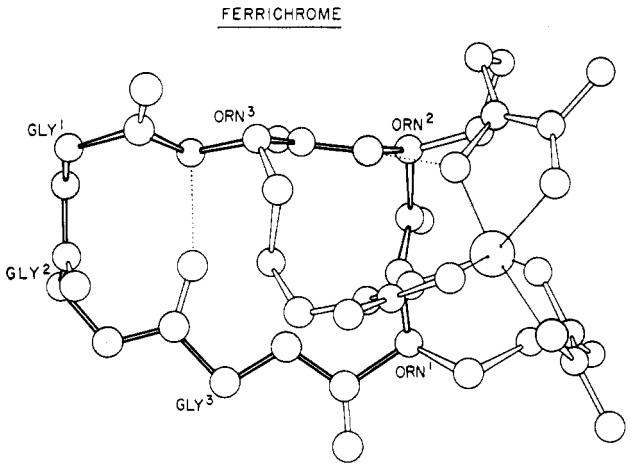

FIGURE 1: Structure of ferrichrome, the ferric coordination derivative of *cyclo*-(Orn^3-Orn^2-Orn^1-Gly^3-Gly^2-Gly^1), where Orn denotes N^δ-acetyl-N^δ-hydroxy-L-ornithine (Zalkin et al., 1966; Llinás et al., 1972; Norrestam et al., 1975). Alumichrome is an isomorphous analogue with Al^{3+} substituting for Fe^{3+}.

used to reconstruct the ^1H spectrum from the ^{13}C spectrum and thus leads to a relative assignment of the coupled heteronuclei (Birdsall et al., 1972).

The alumichrome ^1H NMR spectrum has recently been fully interpreted (De Marco et al., 1978a,b). That information can now be applied to identify totally the aliphatic ^{13}C signals of the peptide on the basis of off-resonance $\{^1H\}^{13}C$ decoupling experiments. Because of its low molecular weight and complex structural features, alumichrome represents a paradigm for polypeptide NMR approaches that can later be applied to larger proteins. The present study revises some of the tentative ^{13}C backbone resonance assignments (Llinás et al., 1977a) and ascribes all the side-chain signals to specific residues. Furthermore, the Orn^1 and Gly^2 carbonyl resonances, essentially degenerate at 25.1 MHz (Llinás et al., 1977b), have now been resolved at the higher field strength and identified by selective $\{^1H\}^{13}C$ decoupling experiments. Heteronuclear $^1J(^1H-^{13}C)$ coupling constants and chemical shifts are reported and discussed in terms of their structural implications for polypeptide ^{13}C NMR studies. A number of $^3J(^1H-^{13}C)$ coupling constants, derived from analyses of the fine structure in the high-resolution ^{13}C spectrum and from comparison of decoupled and undecoupled spectra, are listed. These coupling constants, when related to the known crystallographic dihedral angles, provide a basis to derive a Karplus-type curve for the side-chain χ angles.

Experimental Procedure

The source of the alumichrome peptide has already been described (Llinás et al., 1976a, 1977a). ^{13}C NMR spectra were recorded in the Fourier mode at 67.8846 MHz with an HX-270 Bruker spectrometer ($t \sim 65$ °C, 0.158 M Me_2SO-d_6 solution). Sixteen K data points were used for acquisition, yielding a digital resolution of 0.6 Hz (recycling time of 0.82 s). Rapid accumulation was chosen in order to saturate Me_2SO-d_6 peaks which otherwise would have obscured the undecoupled and off-resonance decoupled spectra where negligible nuclear Overhauser enhancement occurs. As a consequence, slowly relaxing methyl resonances were also somewhat reduced in amplitude.

Five-thousand scans were averaged for the proton broad band decoupled spectrum, while 20 000–100 000 transients were accumulated for the undecoupled and the off-resonance spectra. To achieve sensitivity enhancement, the interferograms were multiplied by a straight line, decreasing from 1.0 to 0.0 between the first and the last data point. Free induction decays were Fourier transformed by using 32K memory size. Sweep width and carrier frequency were matched to have the carbonyl signals aliased but not overlapping with other resonances. The CO region was therefore recorded after reflecting the spectrum. The proton frequencies were measured in the same tube and probe used for the ^{13}C experiments, while advantage was taken of the decoupler coil to transmit the analytical wave.

In order to record the high-resolution undecoupled spectrum shown in Figure 6, we averaged 140 000 scans with a recycling time of 1.03 s (digital resolution = 0.48 Hz). Resolution enhancement was applied by multiplying the interferogram with a parabolic function, which produces effects similar to those obtainable by other techniques (De Marco & Wüthrich, 1976; Wagner et al., 1978). Spectral simulations were performed with the aid of the LAOCN3 computer program (Castellano & Bothner-By, 1964), including, when necessary, the double-resonance Hamiltonian (Becker, 1969; Jikeli et al., 1974).

Table I: Alumichrome ^{13}C Chemical Shifts[a]

	Orn^1	Orn^2	Orn^3	Gly^1	Gly^2	Gly^3
C′	170.49	174.59	169.95	168.24	170.33	169.25
C^α	52.13	58.19	51.89	42.98	44.38	41.20
C^β	25.64	24.32	25.08			
C^γ	21.74	25.98	19.98			
C^δ	47.72	48.68	48.68			
CH_3	(16.16, 15.84, 15.34)[b]					
CO	(161.57, 161.57, 161.96)[b]					

[a] The resonance positions are given in parts per million from internal Me_4Si (Me_2SO-d_6 was assumed at 39.56 ppm). Except for Orn^1 and Gly^2, peptide carbonyl assignments are taken from a previous study (Llinás et al., 1977b). [b] Hydroxamate methyl and carbonyl resonances are not assigned to specific ornithyl residues.

Results

The alumichrome aliphatic ^{13}C NMR spectrum, under conditions of broad-band ^1H decoupling, is shown in Figure 2B. At 67.88 MHz all resonances are resolved except for a pair of transitions which overlap at 48.68 ppm from Me_4Si. The three resonances between 50 and 60 ppm arise from ornithyl α carbons, those between 45 and 50 ppm arise from ornithyl δ carbons, and the ones between 40 and 45 ppm (to lower fields from the Me_2SO multiplet) arise from glycyl α carbons, while the signals between 20 and 30 ppm are due to the six ornithyl β and γ carbons (Llinás et al., 1976a, 1977a). The three closely spaced peaks centered at ~16 ppm arise from the acetyl hydroxamate methyl groups. The complexity which such a spectrum exhibits reflects the unique steric nature of each carbon atom in a structure made rigid by metal coordination.

On switching the ^1H decoupler power off (Figure 2A), the signal intensities are significantly decreased because of the loss of the $\{^1H\}^{13}C$ NOE and because of splitting of the resonances due to the heteronuclear, scalar spin–spin couplings. Thus, e.g., ornithyl C^α resonances become well-defined doublets of $^1J(^1H^\alpha-^{13}C^\alpha) \sim 140$ Hz, each component appearing broadened by smaller longer-range couplings. The resonances from glycyl C^α's and ornithyl side-chain methylene groups appear as pseudotriplets because of two distinct ^1J interactions. The difficulty of dealing with such poorly resolved spectra is exemplified by the region between 15 and 30 ppm. Figure 2 identifies the individual carbon resonances and illustrates their multiplet structures. Assignments, discussed below, are shown in Tables I–IV.

The amide carbonyl ^{13}C transitions occur between 167 and

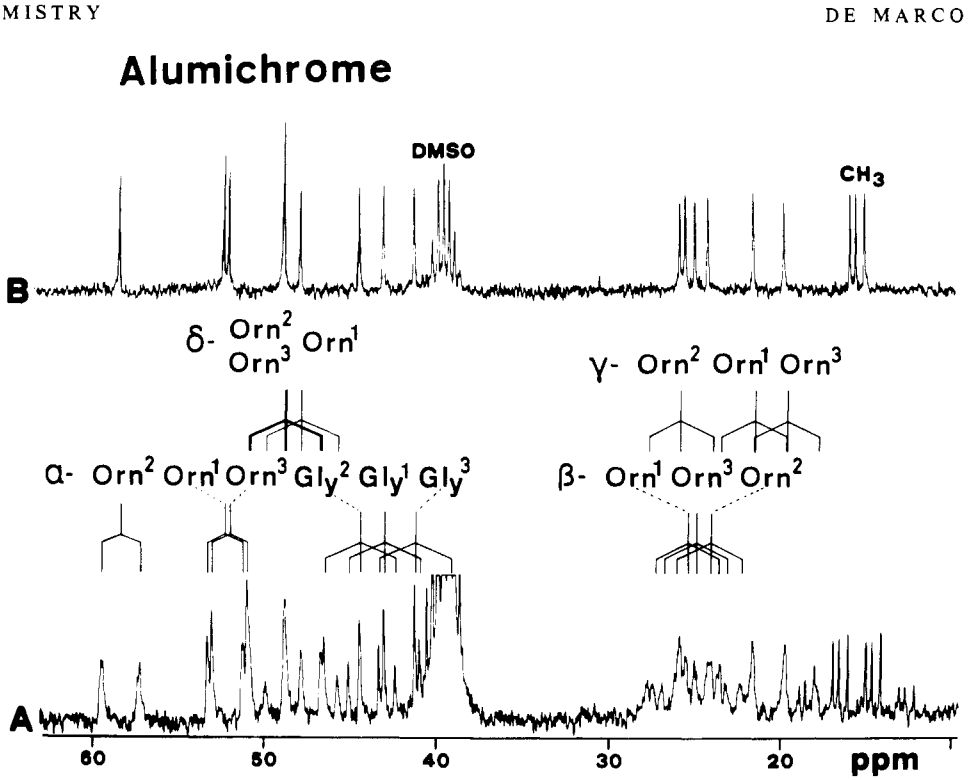

FIGURE 2: High-field region of the ^{13}C NMR spectrum of alumichrome at 67.88 MHz. (A) Undecoupled; (B) with ^{1}H broad-band irradiation. Multiplet structure and resonance assignments are indicated. Acetyl hydroxamate $^{13}CH_3$ signals are not assigned. Me_2SO-d_6 solvent; $t \approx 65$ °C.

Table II: Alumichrome $^{1}J(^{13}C-^{1}H)$ Coupling Constants[a,b]

	Orn^1	Orn^2	Orn^3	Gly^1	Gly^2	Gly^3
C^{α}	137.5	147.0	137.9	139.0	139.0	141.7
C^{β}	126.3	126.0	125.7			
C^{γ}	126.6	126.0	126.3			
C^{δ}	139.6	139.2	139.2			
CH_3	130.0	130.0	130.0			

[a] Coupling constants (in hertz) are all measured as first-order splittings, ±0.5 Hz. [b] The CH_2 triplets in the undecoupled spectrum could not be resolved into doublets of doublets; thus, one heteronuclear coupling is given for both geminal protons.

Table III: Alumichrome $^{3}J(^{13}C-C-C-^{1}H)$ Coupling Constants[a]

	Orn^1	Orn^2	Orn^3
$^{3}J(^{13}C^{\alpha}-C^{\beta}-C^{\gamma}-^{1}H^{\gamma 2})$	0.0[b]	10.4[b]	2.0[b]
$^{3}J(^{13}C^{\alpha}-C^{\beta}-C^{\gamma}-^{1}H^{\gamma 3})$	5.3[b]	5.8[b]	2.5[b]
$^{3}J(^{13}C^{\beta}-C^{\gamma}-C^{\delta}-^{1}H^{\delta 3})$	10.5[c]		11.5[c]
$^{3}J(^{13}C^{\delta}-C^{\gamma}-C^{\beta}-^{1}H^{\beta 2})$	6.5[d]		

[a] Values are given in hertz, ±0.5 Hz. Couplings which could not be confidently estimated from the spectra are left unreported. [b] Measured as splittings in the high-resolution spectrum. The assignments were confirmed by selective heteronuclear double resonance, and the couplings were refined by spectral simulations (Figure 6). [c] Estimated from $^{13}C^{\beta}$ spectra, with and without selective $^{1}H^{\delta 3}$ irradiation. [d] Estimated from $^{13}C^{\delta}$ spectra, with and without selective $^{1}H^{\beta 2}$ irradiation.

175 ppm from Me_4Si (Figure 3D). In contrast to what is observed in the aliphatic region, all $^{13}C{=}O$ resonances present in the broad-band ^{1}H-decoupled spectrum (Figure 3D) maintain their singlet appearance in the ^{1}H-undecoupled spectrum (Figure 3A), where the signals, lacking ^{1}J interactions, are somewhat broadened because of small ^{2}J and ^{3}J couplings to neighbor protons. The unresolved heteronuclear couplings can be removed by low-power ^{1}H irradiation at selected frequencies. Spectra B and C (Figure 3) illustrate two such experiments, where the Orn^1 and Gly^2 $^{1}H^{\alpha}$ transitions are being perturbed. These two carbonyl resonances had not

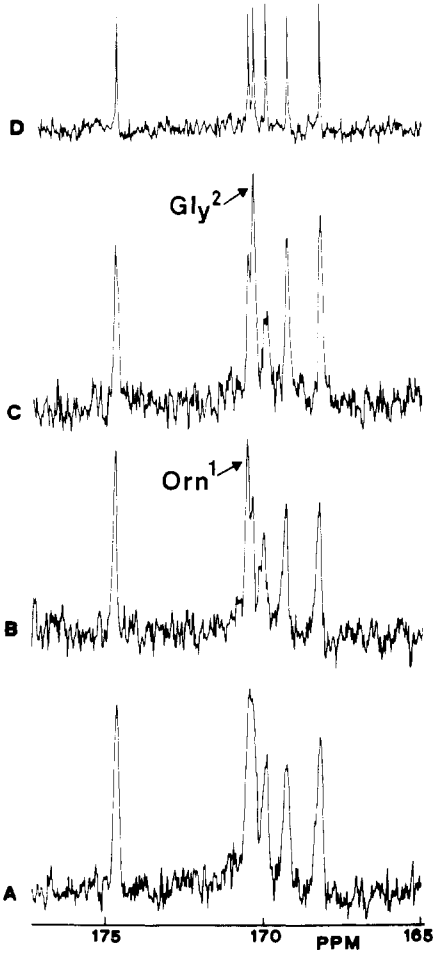

FIGURE 3: Peptide carbonyl region of the ^{13}C NMR spectrum of alumichrome. (A) Undecoupled; (B) irradiation of Orn^1 H^{α} (4.0 ppm); (C) irradiation in the Gly CH_2^{α} region (3.4 ppm); (D) ^{1}H broad-band decoupled spectrum.

Table IV: Intraresidue Carbon-Proton Torsion Angles (deg) for Ferrichrome[a,b]

	Orn[1]	Orn[2]	Orn[3]
$\theta(C^{\alpha}H^{\gamma 2})$	−83	−159	−62
$\theta(C^{\alpha}H^{\gamma 3})$	34	−44	56
$\theta(C^{\beta}H^{\delta 2})$	64	163	63
$\theta(C^{\beta}H^{\delta 3})$	−179	−80	−177
$\theta(C^{\gamma}H^{\alpha})$	52	−58	174
$\theta(C^{\delta}H^{\beta 2})$	34	−43	56
$\theta(C^{\delta}H^{\beta 3})$	−83	−160	−61
$\theta(CO^{\zeta}H^{\delta 2})$[c]	21	−26	4
$\theta(CO^{\zeta}H^{\delta 3})$[c]	−96	−143	−116
$\theta(C'H^{\beta 2})$	−69	−64	57
$\theta(C'H^{\beta 3})$	48	52	174
$\theta(C^{\beta}NH)$	−61	−19	−94
$\theta(C'NH)$	66 (−94[d])	103 (122[e])	30 (16[f])

[a] Based on proton positions determined by proper sp^n hybridization that accounts for nontetrahedral carbon valence configurations (Llinás et al., 1977a) in the X-ray model of the homologues ferrichrome A (Zalkin et al., 1966) and ferrichrysin (Norrestam et al., 1975). Quoted values represent the average between the two available sets of crystallographic data. [b] The relations between the dihedral angles θ and the principal torsion angles are the following: $\theta(C^{\alpha}H^{\gamma 2}) = \chi^2 + 120$; $\theta(C^{\alpha}H^{\gamma 3}) = \chi^2 - 120$; $\theta(C^{\beta}H^{\delta 2}) = \chi^3 + 120$; $\theta(C^{\beta}H^{\delta 3}) = \chi^3 - 120$; $\theta(C^{\gamma}H^{\alpha}) = \chi^1 + 120$; $\theta(C^{\delta}H^{\beta 2}) = \chi^2 - 120$; $\theta(C^{\delta}H^{\beta 3}) = \chi^2 + 120$; $\theta(CO^{\zeta}H^{\delta 2}) = \chi^4 - 120$; $\theta(CO^{\zeta}H^{\delta 3}) = \chi^4 + 120$; $\theta(C'H^{\beta 2}) = \chi^1$; $\theta(C'H^{\beta 3}) = \chi^1 - 120$; $\theta(C'NH) = \varphi \pm 180$, where $\theta(C^{\alpha}H^{\gamma 2,3}) = C^{\alpha}$–$C^{\beta}$–$C^{\gamma}$–$H^{\gamma 2,3}$, etc. These identities are defined for tetrahedral carbons. [c] Corresponds to the hydroxamate carbonyl. [d] Corresponds to Gly^1. [e] Corresponds to Gly^2. [f] Corresponds to Gly^3.

previously been resolved, and their present identification completes the assignments of peptide carbonyl resonances reported elsewhere (Llinás et al., 1977a,b). It is of interest to notice in Figure 3A–C that the Orn^3 $^{13}C'$ resonance at 169.95 ppm is definitely broader than the carbonyl signals from other ornithyl residues. This might be related to the fact that Orn^3 is the only residue whose carbonyl is transoid to a side-chain $^1H^{\beta}$ (Table IV). In fact, this resonance sharpens significantly upon selective irradiation of the Orn^3 $^1H^{\beta 3}$.

Given the close analogy between hydroxamate and backbone amide groups (Llinás et al., 1977b), the ornithyl N^{δ}-hydroxyl-N^{δ}-acetyl methyl groups correspond to $C^{\alpha}H$ groups directly bonded to the peptidyl carbonyl while the $C^{\delta}H$ methylenes model $C^{\alpha}H$'s removed from C′ by one peptide bond. From the spectrum (Figure 4) we estimate that the $^3J(^1H^{\delta}$–$^{13}C')$ is, at most, 4 Hz (assignable to Orn^2, $[\theta] \simeq 143°$, Table IV). In contrast, for the methyl we estimate $^2J(C^1H_3$–$^{13}C') \simeq 6.2$ Hz, consistent with the 6-Hz coupling measured in acetamide (De Marco & Llinás, 1979, and references therein). In enterobactin (Llinás et al., 1973) we concluded that the ^2J due to the amide $^{13}C'$–N–^1H spin–spin interaction is significantly smaller than that due to the similar $^{13}C'$–C^{α}–^1H coupling, the latter being useful for carbonyl assignment by the heteronuclear decoupling technique. The present study on alumichrome confirms these earlier observations and suggests that the method ought to be of general applicability [see also Grathwohl et al. (1973)]. Indeed, we have irradiated the amide protons with a wave centered in the amide region and with enough power to perturb the entire N*H* range, without detecting any significant change in the ^{13}C spectrum. This point deserves careful consideration in view of the unique role played by the amide N*H* resonances to derive peptide conformations. Since the amide $^1H^N$ ^3J coupling to $^{13}C^{\alpha}_{n-1}$ is ~0 Hz for trans peptide bonds (De Marco & Llinás, 1979), it is suggested that while trans peptidyl $^{13}C{=}O$ resonances might be assigned to particular residues on the basis of selective $\{^1H^{\alpha}\}^{13}C'$ decouplings, similar $\{^1H^N\}^{13}C$ experiments are not likely to be as useful.

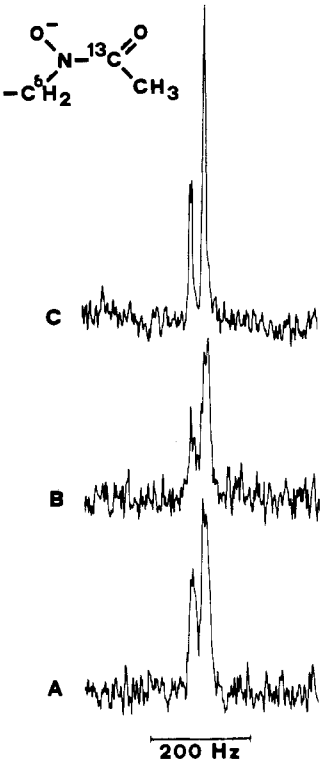

FIGURE 4: Acetyl hydroxamate carbonyl resonances of the ^{13}C NMR spectrum of alumichrome. (A) Undecoupled; (B) under irradiation of the δ protons at 3.4 ppm; (C) under irradiation of the hydroxamate methyl protons at 2.1 ppm. Two of these resonances overlap at 161.57 ppm, the third one appearing at 161.96 ppm.

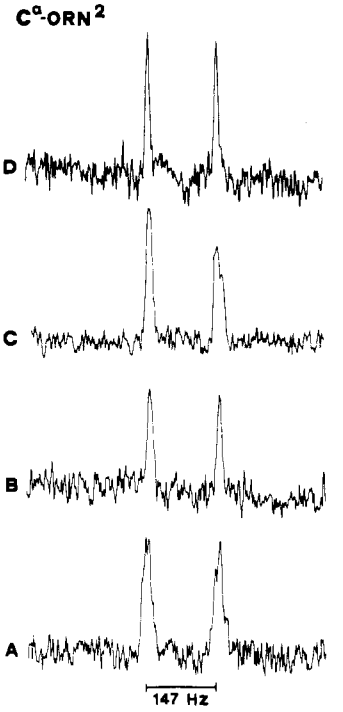

FIGURE 5: Multiplet resonances from Orn^2 $^{13}C^{\alpha}$ of the ^{13}C NMR spectrum of alumichrome under various decoupling conditions. (A) Undecoupled; (B) irradiation at 1.6 ppm, which removes long-range interactions with Orn^2 $H^{\beta 3}$ and $H^{\gamma 3}$; (C) irradiation of Orn^2 $H^{\beta 2}$ at 2.6 ppm; (D) irradiation at 2.0 ppm, very close to the Orn^2 $H^{\gamma 2}$ resonance position.

In contrast to undetected $^3J(^1H^N$–$^{13}C^{\beta})$, steric information is contained in the side-chain heteronuclear couplings. Figure 5A shows the Orn^2 ^{13}C-undecoupled spectrum containing a 147-Hz doublet due to the large, one-bond $^1H^{\alpha}$–$^{13}C^{\alpha}$ spin–spin

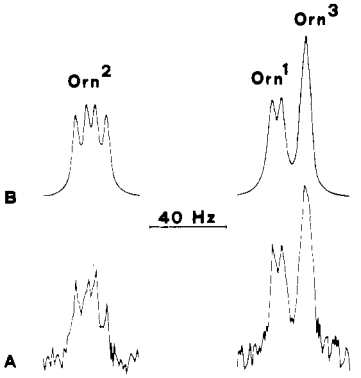

FIGURE 6: Low-field components of the main $^{13}C^{\alpha}$–^{1}H ornithyl doublets in the undecoupled ^{13}C NMR spectrum of alumichrome after resolution enhancement. (A) Experimental, 140 000 scans, resolution-enhanced; (B) simulation. Different peak areas result from the digital filtering.

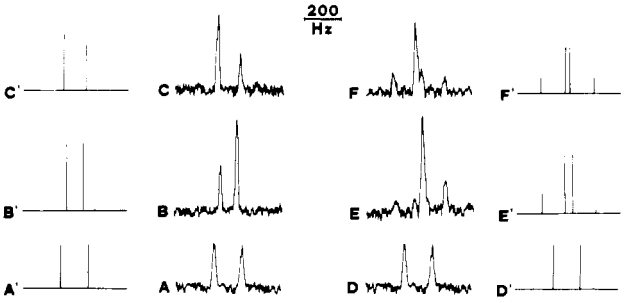

FIGURE 7: Orn^2 $^{13}C^{\alpha}$ multiplet resonances of the ^{13}C NMR spectrum of alumichrome. (A and D) Undecoupled; (B, C, E, and F) $\{^{1}H\}^{13}C$ decoupling experiments, off-resonance from the Orn^2 $^{1}H^{\alpha}$ transition; (A′–F′) stick representations of computer-simulated spectra A–F. The $^{13}C^{\alpha}$ resonances were considered the A part of an AX spin system, where X is the ^{1}J-coupled Orn^2 $^{1}H^{\alpha}$. (B) Irradiation at 4.7 ppm, ~0.6 ppm off-resonance to lower field; (C) irradiation at 3.4 ppm, ~0.7 ppm off-resonance to higher field; (E) irradiation at 4.3 ppm, 0.15 ppm off-resonance to lower field; (F) irradiation at 4.0 ppm, 0.1 ppm off-resonance to higher field.

interaction. Figure 5 illustrates the effect of irradiating the $^{1}H^{\beta 3}$ and $^{1}H^{\gamma 3}$ (Figure 5B), the $^{1}H^{\beta 2}$ (Figure 5C), and the $^{1}H^{\gamma 2}$ (Figure 5D) Orn^2 transitions. It is apparent that $^{3}J(^{1}H^{\gamma}$–$^{13}C^{\alpha}) > {}^{2}J(^{1}H^{\beta}$–$^{13}C^{\alpha})$ and that, significantly, $^{3}J(^{1}H^{\gamma 2}$–$^{13}C^{\alpha}) > {}^{3}J(^{1}H^{\gamma 3}$–$^{13}C^{\alpha})$, which indicates an angular dependence of the heteronuclear 3-bond coupling such that the heteronuclear $^{3}J_{trans} > {}^{3}J_{gauche}$ [for Orn^2 $\chi^2 \simeq 78°$; i.e., $\theta(C^{\alpha}$–$H^{\gamma 2}) \simeq -159°$ and $\theta(C^{\alpha}$–$H^{\gamma 3}) \simeq -44°$ (Table IV)]. Figure 6A displays an expanded, resolution-enhanced spectrum containing low-field components of ornithyl C^{α} multiplets. The three multiplets are readily visualized as varieties of doublets of doublets, suggesting spin–spin interaction with two protons only. Given that in the same spectrum the Gly C^{α} resonances are essentially sharp and unresolved and that aliphatic $^{3}J(^{13}C$–$^{1}H) > {}^{2}J(^{13}C$–$^{1}H)$ [Figure 5; also Tarpley & Goldstein (1971)], the multiplets in Figure 6A can arise only from interactions between C^{α}'s and H^{γ}'s. The splittings, extracted from the spectrum and refined by spectral simulation, are listed in Table III. For Orn^2 $^{3}J(^{13}C^{\alpha}$–$^{1}H^{\gamma 2}) = 10.4$ Hz, which is significantly larger than $^{3}J(^{13}C^{\alpha}$–$^{1}H^{\gamma 3}) = 5.8$ Hz. A few heteronuclear ^{3}J values, related to χ^2 and χ^3, have been estimated from the selective decoupling experiments (Table III).

Thus far, we have concerned ourselves with on-resonance $\{^{1}H\}^{13}C$ decoupling experiments. As mentioned in the beginning of this paper, on-resonance selectivity is difficult to achieve. This is apparent in Figure 3, where even in the favorable case of the carbonyl spectra some perturbation of the Gly^1 (168.2 ppm) and Gly^3 (170 ppm) resonances is apparent when irradiating the Gly^2 $^{1}H^{\alpha}$'s (spectrum C). This is caused by an overlap of the various glycyl α-proton multiplets (De Marco et al., 1978a). A similar effect is discernible in the Orn^2 carbonyl peak at 176.6 ppm when irradiating the Orn^1 $^{1}H^{\alpha}$, but not in the Orn^3 C′ signal at 169.9 ppm because, in this case, the Orn^3 $^{1}H^{\alpha}$ resonance is ~0.6 ppm downfield shifted from the corresponding Orn^1 and Orn^2 $^{1}H^{\alpha}$ transitions (De Marco et al., 1978a). Next, we present features of nonselective $\{^{1}H\}^{13}C$ experiments.

Figure 7 illustrates the Orn^2 C^{α} transitions under full coupling (parts A and D of Figure 7) and partial decoupling (parts B, C, E, and F of Figure 7) conditions. When the $^{1}H^{\alpha}$ wave is about ±0.6 ppm off-resonance, we observe a reduction of the unperturbed 1-bond heteronuclear coupling, J_0, to new values, J_r, which depend on how far to low (Figure 7B) or high (Figure 7C) fields the perturbing ν_2 wave is. In fact, Ernst (1966) has shown that

$$J_r/J_0 = \Delta\nu/(\gamma H_2) \qquad (1)$$

is satisfied for the conditions in parts B and C of Figure 7; i.e., $|\gamma H_2| \gg |\Delta\nu|$ and $|\gamma H_2| \gg |J_0|$, where, if $\nu_x \equiv \nu_{^{1}H}$ on-resonance, $\Delta\nu$ is the offset of the decoupling field, i.e., $\Delta\nu = \nu_2 - \nu_x$, H_2 is the perturbing rf magnetic field at frequency ν_2, and γ is the proton magnetogyric ratio. However, when the perturbing frequency ν_2 is close to ν_x (parts E and F of Figure 7), "spin tickling" conditions are approximated and the ^{13}C spectrum exhibits the four transitions theoretically allowed for such an AX system (Freeman & Anderson, 1962). The computer-simulated stick spectra shown in parts B′, C′, E′, and F′ of Figure 7 ignore intensity variations due to generalized Overhauser effects (Shaw, 1976, and references therein).

The conditions leading to the simple relationship shown in eq 1 are highly restrictive. As Pachler (1972, 1978) has realized, linearity is maintained by using the relation

$$J_r/(J_0^2 - J_r^2)^{1/2} = \Delta\nu/(\gamma H_2) \qquad (2)$$

which is valid under the significantly less limiting conditions $\gamma H_2 \gg {}^{1}/_{2}(J_0^2 - J_r^2)^{1/2}$. Either eq 1 or 2 leads to assignment of coupled heteronuclei.

Simple considerations of chemical shift and signal multiplicities enabled us to divide the alumichrome ^{13}C spectrum into several groups of resonances. The simple criterion "the more off-resonance, the less reduced" was sufficient to follow all the resonances from the undecoupled to the off-resonance decoupled spectrum. We irradiated the proton spectrum of alumichrome at 2.65 ppm, i.e., in the center of the aliphatic proton resonances. Figure 8 shows the result of the experiment. The undecoupled spectrum A is connected to the off-resonance decoupled spectrum B by continuous (α and β carbons) or dashed (γ and δ carbons) lines which allow one to follow each resonance as it shifts under the influence of the decoupling field. In this fashion we could evaluate J_0 and J_r for each $^{1}J(^{1}H$–$^{13}C)$ interaction. Decoupling frequencies, and consequently $\Delta\nu$ for all proton resonances, were measured by recording the proton spectrum using the ^{13}C probe while transmitting the analytical ^{1}H wave via the decoupling coil.

Figure 9A shows the plot of $J_r(J_0^2 - J_r^2)^{-1/2}$ vs. $\Delta\nu$ for the experiment shown in Figure 8. The slope of the least-squares fitted line matches well the strength of the decoupling field γH_2 (in hertz) determined independently. The alignment of the experimental points, marked with different symbols for the various types of carbon atoms, provides convincing evidence that the ^{13}C resonance assignments are correct.

The assignments were verified in two additional experiments performed at lower decoupling power. The irradiation frequency was set at 4.27 and 1.20 ppm, i.e., at about the low- and high-field limits of the aliphatic region of the ^{1}H spectrum, respectively. In the first experiment reduced splittings of Orn

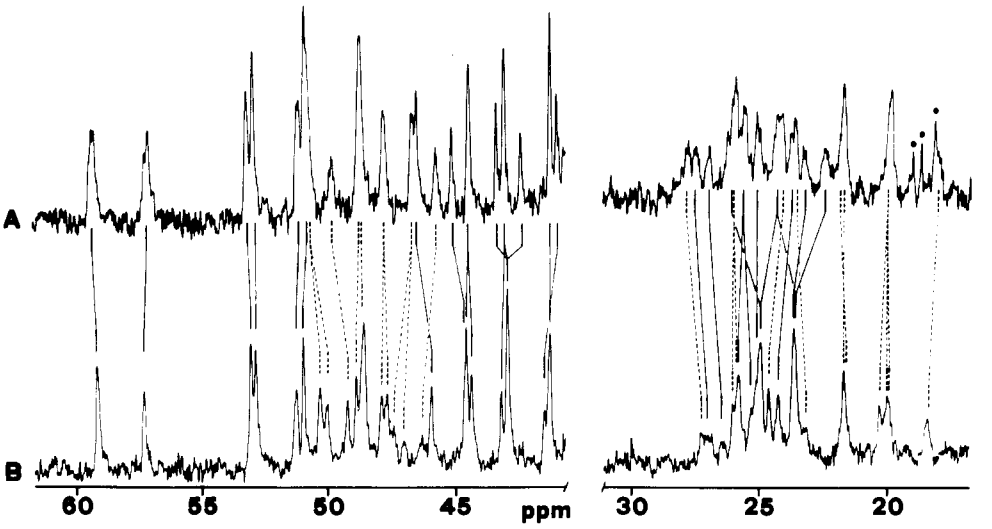

FIGURE 8: ^{13}C NMR spectrum of alumichrome at 67.88 MHz. (A) Undecoupled; (B) single-frequency ^1H irradiation set on the Orn^2 $H^{\beta 2}$ multiplet at 2.65 ppm from Me_4Si. The corresponding resonances in (A) and (B) are connected by solid (Orn C^α and C^β, Gly C^α) and dashed (Orn C^γ and C^δ) lines. The three sharp lines in (A) at ~19 ppm, marked with ●, are the low-field components from CH_3 quartets (see Figure 1). Me_2SO-d_6 solvent; $t \approx 65$ °C.

C^α, Gly C^α, and Orn C^δ were measured, while the latter experiment enabled us to analyze the effect of the irradiation on the ornithyl C^β and C^γ multiplets. The data obtained from the two decouplings, Figure 9B, substantiate the resonance assignments derived from Figure 9A. Figure 2 summarizes the results. Chemical shifts and heteronuclear one-bond coupling constants are reported in Tables I and II, respectively.

Discussion

Resonance Assignments. The assignment of the glycyl α-carbon resonances (Figure 2, Table I) agrees with that previously derived on the basis of comparative NMR studies on homologous peptides (Llinás et al., 1976a, 1977a). The present experiments at a higher magnetic field enable resolution of the two ornithyl $^{13}C^\alpha$ transitions at ~52 ppm and correct the assignment of the Orn^2 (58.19 ppm) and Orn^3 (51.89 ppm) C^α resonances which previously had been identified in reversed order on the basis of a tentative correlation with $^1H^\alpha$ chemical shifts (Llinás et al., 1976a, 1977a). In fact, averaging the chemical shifts for each glycyl geminal α-methylene proton pair [Gly^3, 3.76 ppm; Gly^1, 3.65 ppm; Gly^2, 3.58 ppm (De Marco et al., 1978a)], it is evident that in this case also there is no direct correspondence of $^1H^\alpha$ shifts with the order of appearance of the $^{13}C^\alpha$ resonances. A similar lack of correlation is found for the ornithyl β- and δ-methylene signals. We hence conclude that although a general parallelism is evident between ^1H and ^{13}C spectra in terms of the relative positions of resonances arising from different chemical groups, the trend is not sensitive enough to justify its use as a device to assign resonances to specific amino acid residues in different environments.

Spectral Characteristics. Carbonyl ^{13}C chemical shifts can be relatively well understood on the basis of the extent of hydrogen-bonding donor or acceptor role of the amide groups (Llinás et al., 1977b). Unfortunately, even an approximate theory is lacking to deal with the NMR frequencies of aliphatic carbons or, for that matter, of their covalently linked hydrogens. No attempt shall be made here to rigorously rationalize the ^{13}C spectral pattern exhibited by the alumichrome aliphatic groups. However, there are trends in the data, indicative of polarization effects transmitted to the α carbons from the amide groups, which merit discussion.

Formally, it is possible to extend the amide dipolar resonance forms to other canonical species where electron density

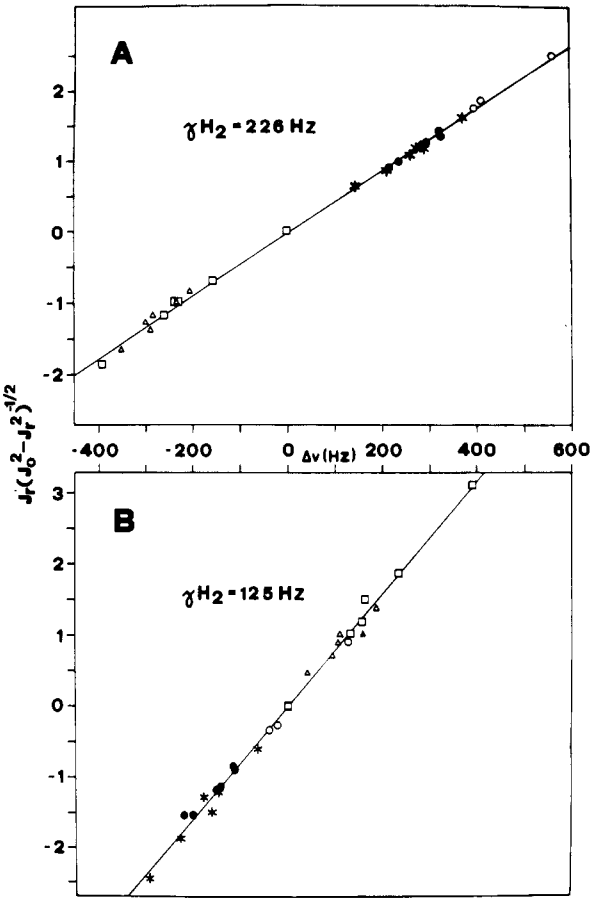

FIGURE 9: Pachler plots for off-resonance $\{^1H\}^{13}C$ decoupling experiments on alumichrome. (A) Experiment shown in Figure 8; the decoupling power γH_2 is 226 Hz. (B) Results from two experiments at lower decoupling power (γH_2 = 125 Hz) where the decoupling ^1H frequencies are set at 1.20 and 4.27 ppm from Me_4Si. (●) Gly$^\alpha$; (○) Orn$^\alpha$; (□) Orn$^\beta$; (△) Orn$^\gamma$; (*) Orn$^\delta$. Straight lines represent linear least-squares fits of the experimental data points based on the equation $\Delta\nu = \gamma H_2 J_r (J_0^2 - J_r^2)^{-1/2}$ (Pachler, 1972).

deficiency at the peptide bond is delocalized to attached C^α's. As discussed elsewhere (Llinás & Klein, 1975; Llinás et al., 1976b, 1977b), the stability of A relative to B (Scheme I) is controlled by the peptide group role as hydrogen-bond acceptor (>C=O···H–) or donor (>:N–H···O=). Based on the

Scheme I

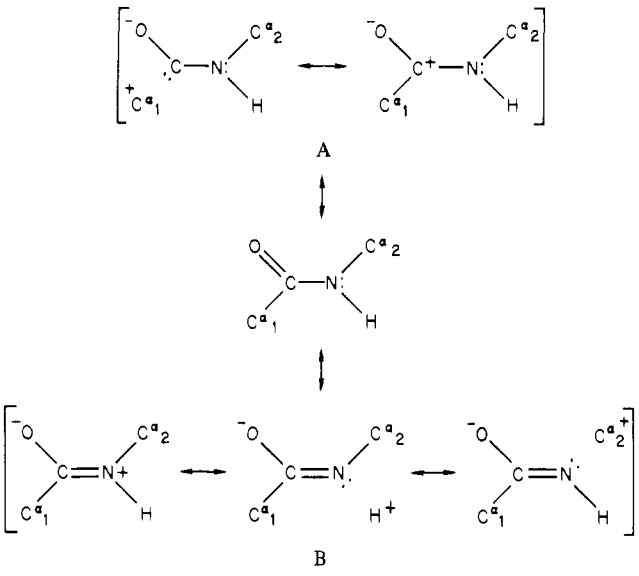

crystallographic model for other ferrichromes (Zalkin et al., 1966; Norrestam et al., 1975) and the heteronuclear NMR data of alumichrome (Llinás & Klein, 1975; Llinás et al., 1976b, 1977b), Gly^3 is the only residue whose carbonyl is intramolecularly hydrogen bonded, to the Orn^3 amide, while its own NH is essentially internal, providing negligible hydrogen bonding (Figure 1). Carbonyl groups of the other residues all point "out" toward the solvent, Me_2SO, that affords a nonprotic environment.

Extensive ^{13}C NMR literature indicates that electron-withdrawing substituents tend to increase the magnitude of the methyl $^1J(^1H-^{13}C)$ (Stothers, 1972, and references therein). Thus, e.g., on going from $^-O-CH_3$ to $H_2{}^+O-CH_3$ there is a 27-Hz increase in the heteronuclear ^1J. Similarly, it has been observed that in carbonium ions ^1J increases by 7–10 Hz in methyl groups adjacent to the positive carbon, regardless of the nature of the other atoms bound to the cationic center. Because its carbonyl is intramolecularly hydrogen bonded, canonical structures A (Scheme I) should be relatively favored for Gly^3, which implies a partial hole delocalization toward its $C^{\alpha}{}_1$. This might explain why the Gly^3 $^1J(^1H-^{13}C^{\alpha})$ is 2.7 Hz larger than in Gly^1 or Gly^2, whose heteronuclear $^1J^{\alpha}$ values are similar to those measured for Orn^1 and Orn^3, i.e., 139.0 vs. 137.5 and 137.9 Hz, respectively (Table II). In comparison, Orn^2 exhibits $^1J(^1H-^{13}C^{\alpha})$ = 146.0 Hz, i.e., more than 8 Hz larger than for Orn^1 or Orn^3. As shown by the model (Figure 1), the Orn^2 NH is involved in a very strong hydrogen bond to its own hydroxamate N–O^- group (crystallographic Orn^2–N···O–N distance = 2.80 Å; Zalkin et al., 1966) which would favor canonical structures B. For such a case abundant data also exist indicating an increase in the magnitude of $^1J(^1H-^{13}C)$ (Stothers, 1972). Thus, e.g., in going from H_2N-CH_3 to $H_3N^+-CH_3$, the methyl ^1J increases by 12 Hz, a change which is consistent with the ~8-Hz larger magnitude of the Orn^2 $^1J^{\alpha}$.

The strong Orn^2 hydrogen bond would explain the extreme low-field position of its $^{13}C^{\alpha}$ resonance, ~6 ppm more deshielded than the corresponding signals of both Orn^1 and Orn^3 (Table I). However, this would not explain the high-field $^{13}C^{\alpha}$ resonance shift of Gly^3 relative to Gly^1 and Gly^2. As reported elsewhere (Llinás et al., 1977b), Gly^3 and Orn^3 both exhibit significant tetrahedral distortions at C^{α}, describing bond angles which formally yield bond orbital hybridizations of $sp^{1.49}$ for the first and $sp^{1.65}$ for the second. Empirical correlations show that relative to sp^3 carbons, sp^2 carbons resonate at ~100 ppm toward lower fields while sp hybrids appear in the spectrum between sp^3 and sp^2 positions. Hence, it is not unlikely that the lower hybridizations of Gly^3 and Orn^3 C^{α}'s tend to shift their resonances toward somewhat different positions than those shown by their homologous residues. Similarly, as judged from the crystallographic coordinates, Gly^1 and Gly^2 C^{α}'s are better described by $sp^{2.39}$ and $sp^{2.25}$ hybrid orbitals, respectively, while for the homologous atom in Orn^1 and Orn^2 one would formally assign $sp^{2.65}$ and $sp^{2.13}$ configurations, respectively (Llinás et al., 1977a). Thus, the extreme low-field position of the Orn^2 C^{α} might be contributed to by its olefin-like s character. On analogous grounds, Gly^2 and Gly^1 α resonances should appear in that order on going from low to high fields, which is what is observed, while the corresponding Gly^3 signal should be at an even higher field position, opposing the polarization effect discussed above. The fact that the Orn^3 C^{α} appears somewhat low-field shifted relative to its hybridization can thus be accounted for in terms of a partial deshielding caused by its weak, donor hydrogen bonding to the Gly^3 carbonyl (Figure 1).

It is of interest to notice (a) the lack of magnetic equivalence of the hydroxamate carbonyl groups (Figure 4, Table I) and (b) the spread of methyl chemical shifts (Figure 2, Table I). This effect, although minor when compared with what is observed at backbone sites, is similarly transmitted to the ornithyl side-chain carbons. The C^{β}, C^{γ}, and C^{δ} resonances are hence simultaneously subject to inductive effects arising from electron-labile groups at both ends of the side chain and to the type of hybridization shifts discussed above for the C^{α}'s. It is observed that while the C^{β}'s and C^{δ}'s each span ~1 ppm, the C^{γ} resonances spread over a 6-ppm range (Figure 2, Table I). Furthermore, the methylene one-bond heteronuclear couplings are essentially identical for β and γ carbons, $^1J \simeq$ 126 Hz, i.e., considerably smaller than those for the C^{δ} resonances that yield ^1J ~139 Hz triplets, the splitting being similar in magnitude to those exhibited by the backbone α carbons (Table II), consistent with the amide character of the hydroxamate group. In comparison, the hydroxamate methyl groups exhibit ^1J = 130.0 Hz, close to ^1J = 129 Hz in acetamide (Stothers, 1972).

In summary, we conclude that the chemical shift and $^1J(^{13}C-^1H)$ spectral characteristics of peptide ^{13}C resonances are determined by (a) inductive effects peculiar to each amino acid side-chain substituent, (b) local orbital hybridizations that account for the strained peptide conformation, and (c) electron density deficiencies originating at hydrogen-bonded peptidyl amides and metal-binding sites. *Conclusions b and c merit special attention as there has been a tendency to ascribe "unusual" aliphatic ^{13}C chemical shifts to ring current anisotropies from aromatic side chains. Alumichrome clearly indicates that such need not always be the case.*

$^1H-^{13}C$ Spin–Spin Couplings. The six vicinal $^{13}C^{\alpha}-^1H^{\gamma}$ coupling constants, measured in the undecoupled resolution-enhanced C^{α} multiplets (Figure 6, Table III), are related to side-chain dihedral angles, corresponding to the conventional, principal torsion angles χ^2 (Table IV). The stereospecific assignments given in Table III stem from decoupling experiments of the type exemplified in Figure 5 and are also based on the assumption that the ^3J values follow a Karplus-type trend. Table IV shows that the six $\theta(C^{\alpha}-H^{\gamma})$'s cover a wide domain of dihedral angles, from ~30 to ~160° (quasi-trans), a range in which two gauche situations ($H^{\gamma 2}$ and $H^{\gamma 3}$ Orn^3) and the usual "minimum" conformation (−83°, $H^{\gamma 2}$ Orn^1) are represented. For this reason, even though only six

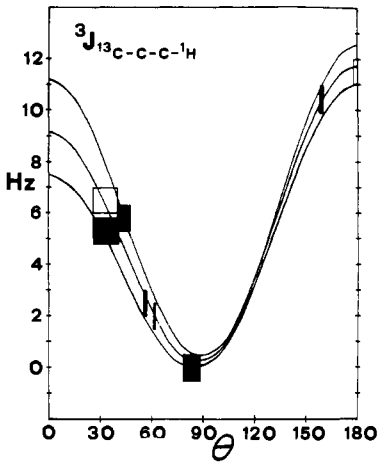

FIGURE 10: Karplus curve for the vicinal ^{13}C–^1H coupling constants. The data represent the six couplings derived from the $^{13}C^{\alpha}$ ornithyl resonances shown in Figure 6 (closed rectangles). Also included are the three values provided by the ornithyl $^{13}C^{\beta}$ and $^{13}C^{\delta}$ resonances (open rectangles: two coincide at $\theta \approx 170°$, see Table III). The fit was performed only on the six $^{13}C^{\alpha}$–$^1H^{\gamma}$ coupling constants. The vertical dimension represents the NMR uncertainty (±0.5 Hz for all points, see Table III), while horizontally the rectangles span a θ range limited by the two sets of available crystallographic data (Zalkin et al., 1966; Norrestam et al., 1975).

pairs of ^3J–θ values are available, we can confidently fit the data to a Karplus curve, obtaining eq 3. Equation 3 is plotted

$$^3J(\theta) = (10.2 \pm 0.9)\cos^2\theta - (1.3 \pm 1.2)\cos\theta + (0.2 \pm 0.2)\text{ Hz} \quad (3)$$

in Figure 10 together with the estimated limits of confidence. The root mean square error for the polynomial regression of ^3J vs. cos θ is 0.7 Hz. The closed rectangles in Figure 10 represent the six pairs of ^3J–θ data points used for the fit. Open rectangles represent the three additional ^3J values related to χ^2 and χ^3 (Table III), estimated from comparison of undecoupled and selectively decoupled spectra (two rectangles coincide at $\theta \sim 180°$). The fact that the latter points fit well on the curve obtained for χ^2 suggests that, as for the proton–proton couplings (De Marco et al., 1978a), the proton–carbon vicinal interactions related to χ^1, χ^2, χ^3, etc. fit a single Karplus equation.

Equation 4, obtained by INDO MO calculations on the

$$^3J(\theta) = 4.26 - 1.00\cos\theta + 3.56\cos 2\theta\text{ Hz} \quad (4)$$

^{13}C–C–C–H fragment in propane, has been proposed by Wasylishen & Schaefer (1972). It can be rewritten as eq 5.

$$^3J(\theta) = 7.12\cos^2\theta - 1.00\cos\theta + 0.70\text{ Hz} \quad (5)$$

Equation 4 or 5 yields $J_{gauche} = 2.0$ Hz, $J_{trans} = 8.8$ Hz, and an average coupling constant for free rotation $J_{av} = 4.3$ Hz. If these couplings are compared with the values derived from eq 3, $J_{gauche} = 2.1$ Hz, $J_{trans} = 11.7$ Hz, and $J_{av} = 5.3$ Hz, it is noticed that although the curve we propose is slightly steeper than the theoretical curve, the values do not differ significantly once the experimental uncertainties are accounted for. Similarly, reported studies on uridine (Lemieux et al., 1972; Delbaere et al., 1973; Lemieux, 1973) and carbohydrates (Schwarcz & Perlin, 1972) conclude that $^3J(60°) \sim 2$ Hz and $^3J(180°) \gtrsim 8$ Hz. Equation 3 thus represents the first instance in which a quantitative dependence of ^{13}C–C–C–^1H coupling constants on the related dihedral angle has been directly established from correlation of experimental NMR data on a structure with well-defined conformational parameters. Such a relation should be useful in solving the ambiguity that arises in the determination of torsion angles when side-chain diastereotopic methylene protons are not stereochemically assigned. This is particularly important for side-chain torsion angles beyond the β position, a case for which complementary data such as $^3J(^1H^{\beta}$–$^{13}C')$ (Hansen et al., 1975; Espersen & Martin, 1976) or $^3J(^1H^{\beta}$–$^{15}N)$ (De Marco et al., 1978c) are not available.

Acknowledgments

The authors are indebted to Professor P. M. McCurry, Jr., for reading the manuscript and for valuable suggestions.

References

Becker, E. D. (1969) *High Resolution NMR*, Academic Press, New York.
Birdsall, B., Birdsall, N. J. M., & Feeney, J. (1972) *J. Chem. Soc., Chem. Commun.*, 316–317.
Castellano, S., & Bothner-By, A. A. (1964) *J. Chem. Phys. 41*, 3863–3869.
Delbaere, L. T. J., James, M. N. G., & Lemieux, R. U. (1973) *J. Am. Chem. Soc. 95*, 7866–7868.
De Marco, A., & Wüthrich, K. (1976) *J. Magn. Reson. 24*, 201–204.
De Marco, A., & Llinás, M. (1979) *Org. Magn. Reson.* (in press).
De Marco, A., Llinás, M., & Wüthrich, K. (1978a) *Biopolymers 17*, 617–636.
De Marco, A., Llinás, M., & Wüthrich, K. (1978b) *Biopolymers 17*, 637–650.
De Marco, A., Llinás, M., & Wüthrich, K. (1978c) *Biopolymers 17*, 2727–2742.
Dill, K., & Allerhand, A. (1977) *Biochemistry 16*, 5711–5716.
Ernst, R. R. (1966) *J. Chem. Phys. 45*, 3845–3861.
Espersen, W. G., & Martin, R. B. (1976) *J. Phys. Chem. 80*, 741–745.
Freeman, R., & Anderson, W. A. (1962) *J. Chem. Phys. 37*, 2053–2073.
Grathwohl, Ch., Schwyzer, R., Tun-Kyi, A., & Wüthrich, K. (1973) *FEBS Lett. 29*, 271–274.
Hansen, P. E., Feeney, J., & Roberts, G. C. K. (1975) *J. Magn. Reson. 17*, 249–261.
Jikeli, G., Herrig, W., & Günther, H. (1974) *J. Am. Chem. Soc. 96*, 323–324.
Komoroski, R. A., Peat, I. R., & Levy, G. C. (1976) *Top. Carbon-13 NMR Spectrosc. 2*, 179–267.
Lemieux, R. U. (1973) *Ann. N.Y. Acad. Sci. 222*, 915.
Lemieux, R. U., Nagabhushan, T. L., & Paul, B. (1972) *Can. J. Chem. 50*, 773–776.
Llinás, M., & Klein, M. P. (1975) *J. Am. Chem. Soc. 97*, 4731–4737.
Llinás, M., Klein, M. P., & Neilands, J. B. (1972) *J. Mol. Biol. 68*, 265–284.
Llinás, M., Wilson, D. M., & Neilands, J. B. (1973) *Biochemistry 12*, 3836–3843.
Llinás, M., Wilson, D. M., Klein, M. P., & Neilands, J. B. (1976a) *J. Mol. Biol. 104*, 853–864.
Llinás, M., Horsley, W. J., & Klein, M. P. (1976b) *J. Am. Chem. Soc. 98*, 7554–7558.
Llinás, M., Wilson, D. M., & Neilands, J. B. (1977a) *J. Am. Chem. Soc. 99*, 3631–3637.
Llinás, M., Wilson, D. M., & Klein, M. P. (1977b) *J. Am. Chem. Soc. 99*, 6846–6850.
Norrestam, R., Stensland, B., & Brändén, C. I. (1975) *J. Mol. Biol. 99*, 501–506.
Norton, R. S., & Allerhand, A. (1976) *Biochemistry 15*, 3438–3445.
Oldfield, E., Norton, R. S., & Allerhand, A. (1975) *J. Biol. Chem. 250*, 6381–6402.

Pachler, K. G. R. (1972) *J. Magn. Reson. 7*, 442–443.
Pachler, K. (1978) *J. Magn. Reson. 32*, 177.
Packer, E. L., Sternlicht, H., Lode, E. T., & Rabinowitz, J. C. (1975) *J. Biol. Chem. 250*, 2062–2072.
Schwarcz, J. A., & Perlin, A. S. (1972) *Can. J. Chem. 50*, 3667–3676.
Shaw, D. (1976) in *Fourier Transform NMR Spectroscopy*, Chapter 9, Elsevier, Amsterdam.
Sogn, J. A., Craig, L. C., & Gibbons, W. A. (1974) *J. Am. Chem. Soc. 96*, 3306–3309.
Stothers, J. B. (1972) *Carbon-13 NMR Spectroscopy*, Academic Press, New York.
Tanabe, M., Hamasaki, T., Thomas, D., & Johnson, L. F. (1971) *J. Am. Chem. Soc. 93*, 273–274.
Tarpley, A. R., Jr., & Goldstein, J. H. (1971) *J. Am. Chem. Soc. 93*, 3573–3578.
Wagner, G., Wüthrich, K., & Tschesche, H. (1978) *Eur. J. Biochem. 86*, 67–76.
Wasylishen, R., & Schaefer, T. (1972) *Can. J. Chem. 50*, 2710–2712.
Wilbur, D. J., & Allerhand, A. (1977) *J. Biol. Chem. 252*, 4969–4975.
Zalkin, A., Forrester, J. D., & Templeton, D. H. (1966) *J. Am. Chem. Soc. 88*, 1810–1814.

Partial Characterization of a Tropoelastin Precursor Isolated from Chick Aorta†

Robert B. Rucker,* Chor San Heng-Khoo, Michael Dubick, Michael Lefevre, and Carroll E. Cross

ABSTRACT: Evidence is presented that indicates tropoelastin is derived from a soluble elastin with a molecular weight of 95 000. Tropoelastin and its proposed precursor were isolated from the aortas of copper-deficient chicks. Although it is doubtful that the proposed precursor is an initial product of elastin translation, i.e., a proelastin, it is proposed to be at least a truncated form of proelastin that is converted to tropoelastin. The key to its isolation was the presence of α_1-antitrypsin at each step in the purification procedure. The first 11 amino acid residues at the NH_2 terminal of the proposed tropoelastin precursor (GGVPGAVPGGV) are the same as those for tropoelastin. Its amino acid composition is similar to that of tropoelastin, except for higher amounts of acidic amino acid residues. Further, the proposed precursor contains a limited number of aldehydic functions, presumably in the form of peptidyl allysine. This was taken as an indication that the proposed precursor serves as a substract for lysyl oxidase. Under the conditions used for the isolation, the precursor appeared to be in higher concentrations than tropoelastin in aorta extracts from copper-deficient chicks.

Tropoelastin is a soluble elastin with a molecular weight of ~72 000. It is generally accepted as the precursor to insoluble elastin, a highly cross-linked structural protein with the physical properties of an elastomer (Sandberg, 1976; Rucker & Tinker, 1977). Although there are reports that suggest tropoelastin is the only form of elastin secreted by cells capable of synthesizing elastin (Ryhänen et al., 1978; Burnett & Rosenbloom, 1979), Foster et al. (1977, 1978) have provided evidence for a soluble proelastin that appears modified to tropoelastin. They suggest that the molecular weight of proelastin is 120 000–140 000 (Foster et al., 1977). In comparison to tropoelastin, it contains more acidic and hydroxy amino acid residues. It also appears to contain histidine, cysteine, and methionine, i.e., amino acids typically not found in tropoelastin. Foster et al. (1977, 1978) isolated the proelastin from the aortas of lathyritic chicks. An important feature of their isolation was the use of high concentrations of proteolytic inhibitors. Without the use of proteolytic inhibitors during isolation, the predominant product was tropoelastin.

Using chicks fed copper-deficient diets, we have also reported the isolation of tropoelastin from chick aorta (Rucker et al., 1975) identical with the tropoelastin described by Foster et al. (1975). Both nutritional copper deficiency and lathyrism decrease cross-linking of insoluble elastin, which is necessary in order to isolate soluble elastins in quantities sufficient for characterization. Although we have yet to isolate a proelastin from the aorta of copper-deficient birds, the use of procedures similar to those described by Foster et al. (1977) resulted in the isolation of a soluble elastin with a molecular weight of 90 000–100 000. We feel that this form of soluble elastin may be an intermediate in the modification of proelastin to tropoelastin. This view is not inconsistent with that of Foster et. al. (1978), and it is in keeping with our previously reported observations on forms of soluble elastins which were identified by using radiochemical labeling procedures (Heng-Khoo et al., 1979; Rucker et al., 1977).

To be described are some of the properties of the proposed intermediate to tropoelastin. This form of soluble elastin possesses an amino acid composition similar to that of tropoelastin. Data obtained from amino acid sequencing indicate that its first 11 NH_2-terminal amino acid residues are identical with those of tropoelastin. Although the exact role of the proposed intermediate in elastin fibrogenesis is not clear, it does appear to be a predominant form of soluble elastin in aortas from copper-deficient chicks. This is an important point since for all previous reports using aortas from copper-deficient animals as a soluble elastin source only tropoelastin has been observed to be the predominant form in tissue extracts [cf. Rucker & Tinker (1977) and Sandberg (1976) and references cited therein].

† From the Department of Nutrition, College of Agricultural and Environmental Sciences, and the Department of Pulmonary Medicine, School of Medicine, University of California, Davis, California 95616. *Received March 23, 1979.* Supported by U.S. Public Health Service Grants No. HL-15965 and HL-18918 from the National Institute for Heart and Lung. M.L. receives support from a training grant (DE-07001, National Institute of Dental Research). M.D. is supported by a grant from the Parker Francis Foundation.

* Address correspondence to the Department of Nutrition.

0006-2960/79/0418-3854$01.00/0